Supporting Information

Structural, magnetic and phase transition properties in S = ½ radical solid solutions of $[F_xCl_{1-x}\text{-BzPy}][Ni(mnt)_2]$ (x = 0.07–0.87)

Wan-Wan Yao,[a] Bin-Bin Ma,[a] Lei Xu,[a] Dong-Sheng Shao,[a] Yin Qian,[a]* Wen-Long Liu,[b] Xiao-Ming Ren*[a,c,d]

[a] State Key Laboratory of Materials-Oriented Chemical Engineering and College of Chemistry and Molecular Engineering, Nanjing Tech University, Nanjing 211816, P. R. China

[b] College of Chemistry and Chemical Engineering, Yangzhou University, Yangzhou 225002, P. R. China

[c] College of Materials Science and Engineering, Nanjing Tech University, Nanjing 211816, P. R. China

[d] State Key Laboratory of Coordination Chemistry, Nanjing University 210023, P. R. China

Email: yinqian@njtech.edu.cn (YQ); xmren@njtech.edu.cn (XMR)

Contents

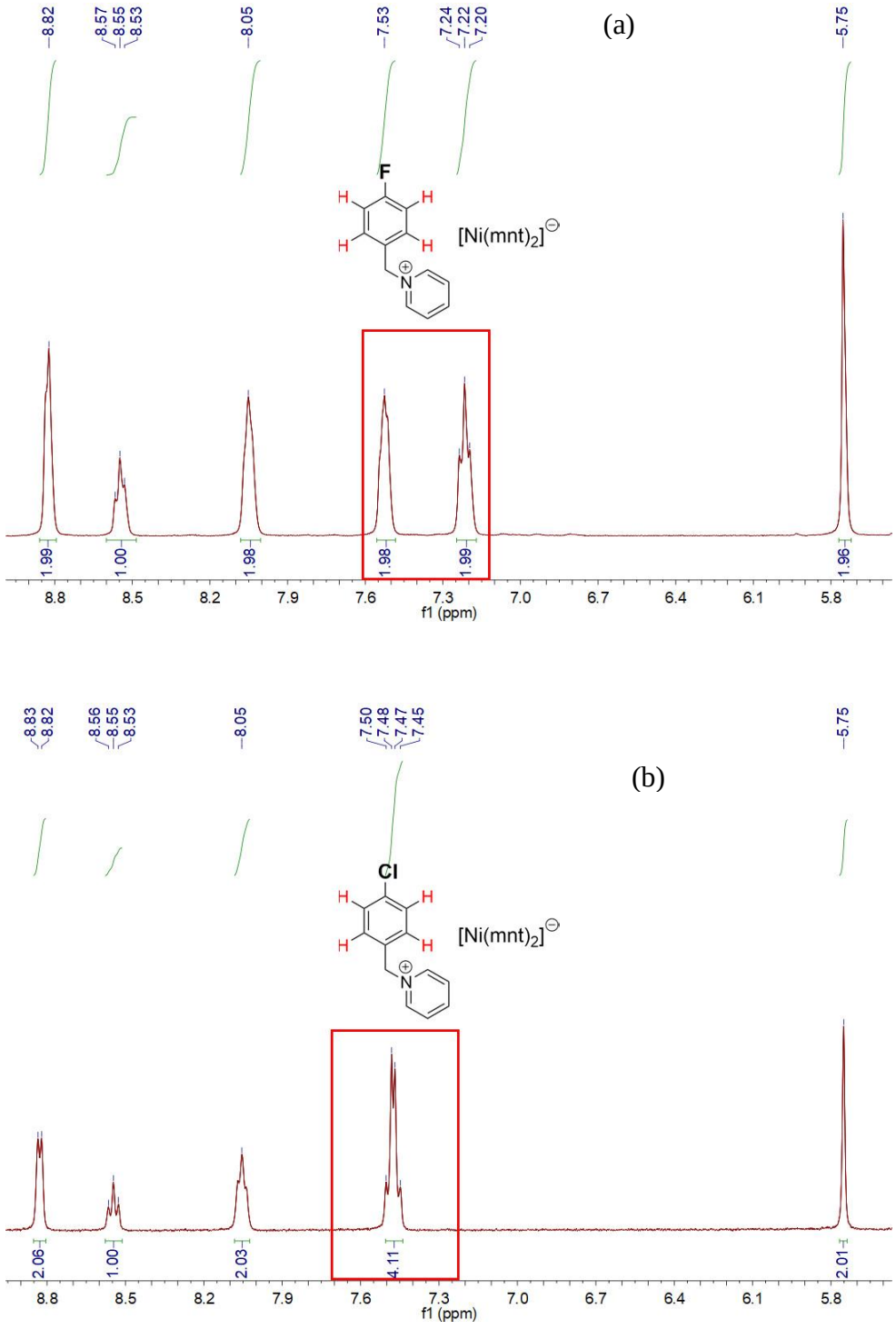

Fig. S1: ^{1}H NMR spectra of (a) [F-BzPy][Ni(mnt)$_2$] and (b) [Cl-BzPy][Ni(mnt)$_2$].

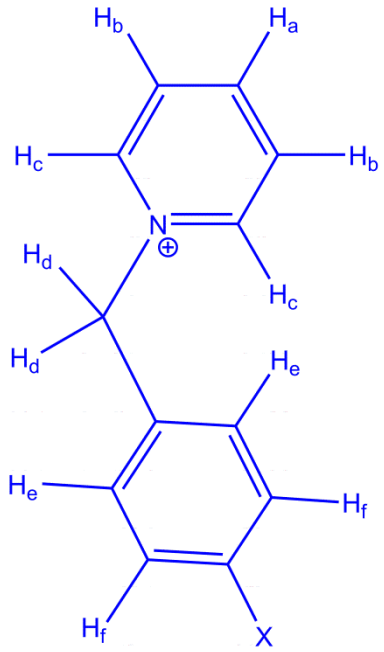

(X = F or Cl)

Fig. S2: Schematic illustration of different chemical environments of hydrogen atoms in X-BzPy^{+} (X = F or Cl) cation.

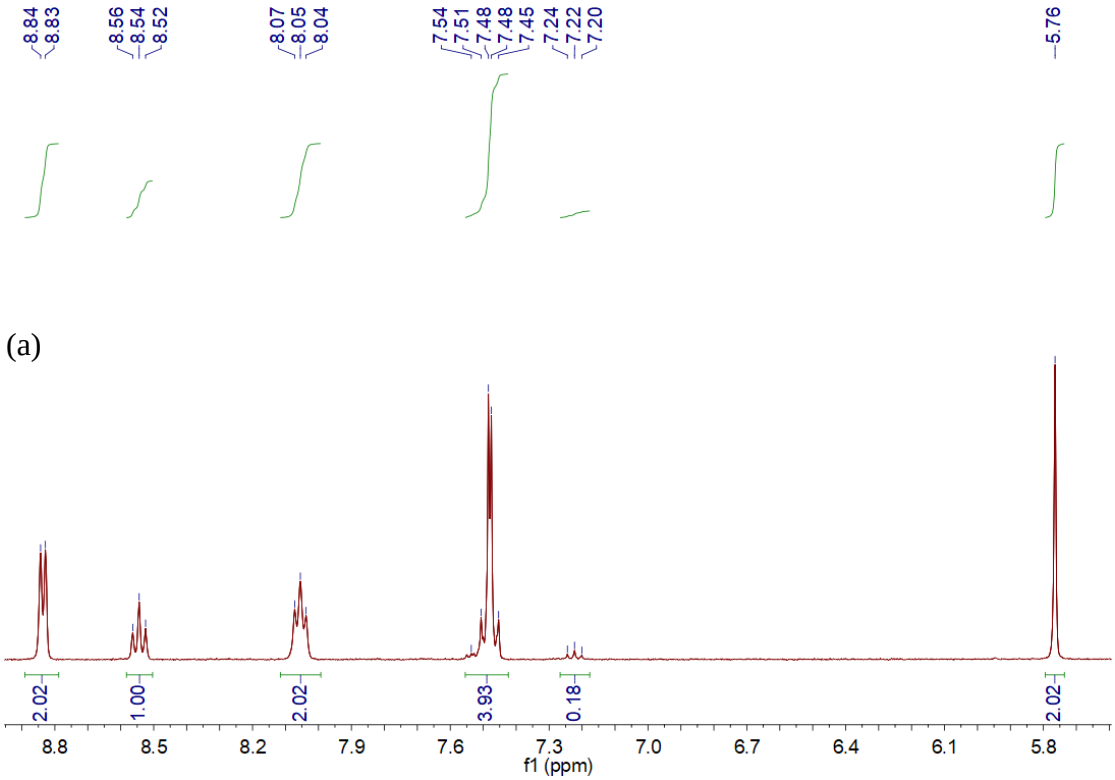
8.84
8.83
8.56
8.54
8.52
8.07
8.05
8.04
7.54
7.51
7.48
7.48
7.45
7.24
7.22
7.20
5.76
2.02
1.00
2.02
3.93
0.18
2.02
8.8
8.5
8.2
7.9
7.6
7.3
7.0
6.7
6.4
6.1
5.8
f1 (ppm)

(a)

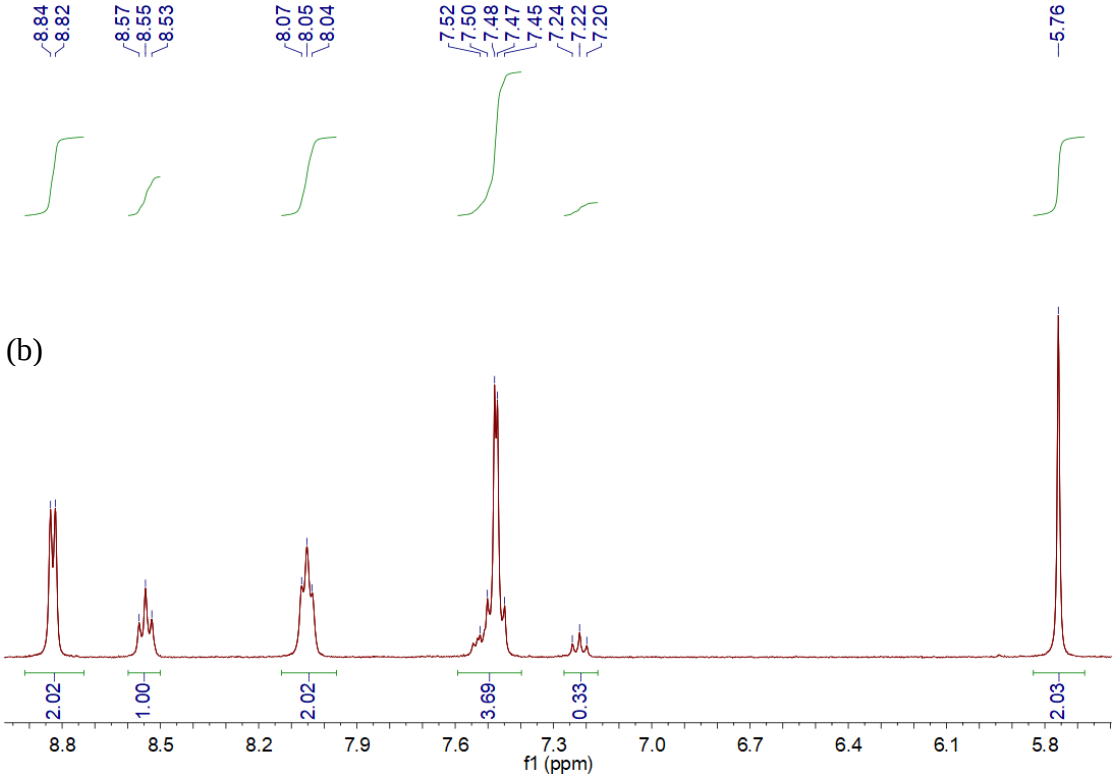
8.84
8.82
8.57
8.55
8.53
8.07
8.05
8.04
7.52
7.50
7.48
7.47
7.45
7.24
7.22
7.20
5.76
2.02
1.00
2.02
3.69
0.33
2.03
8.8
8.5
8.2
7.9
7.6
7.3
7.0
6.7
6.4
6.1
5.8
f1 (ppm)

(b)

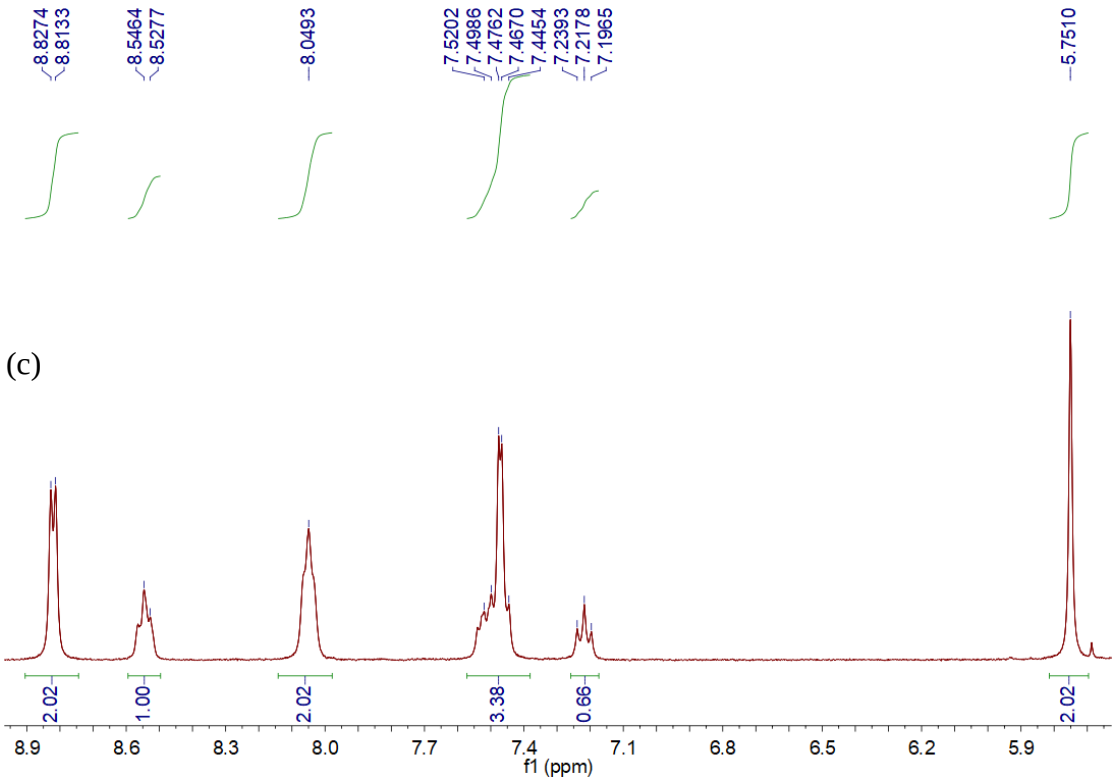
8.8274
8.8133
8.5464
8.5277
8.0493
7.5202
7.4986
7.4762
7.4670
7.4454
7.2393
7.2178
7.1965
5.7510
2.02
1.00
2.02
3.38
0.66
2.02
8.9
8.6
8.3
8.0
7.7
7.4
7.1
6.8
6.5
6.2
5.9
f1 (ppm)

(c)

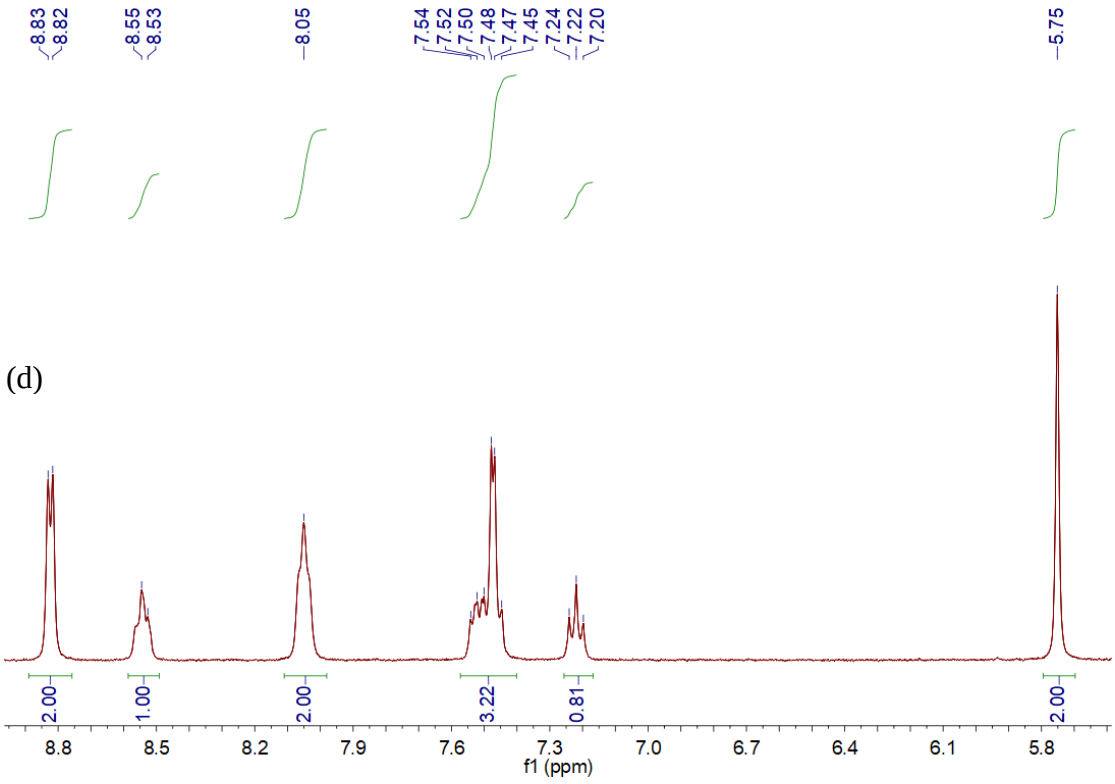
8.83
8.82
8.55
8.53
8.05
7.54
7.52
7.50
7.48
7.47
7.45
7.24
7.22
7.20
5.75
2.00
1.00
2.00
3.22
0.81
2.00
8.8
8.5
8.2
7.9
7.6
7.3
7.0
6.7
6.4
6.1
5.8
f1 (ppm)

(d)

(e)

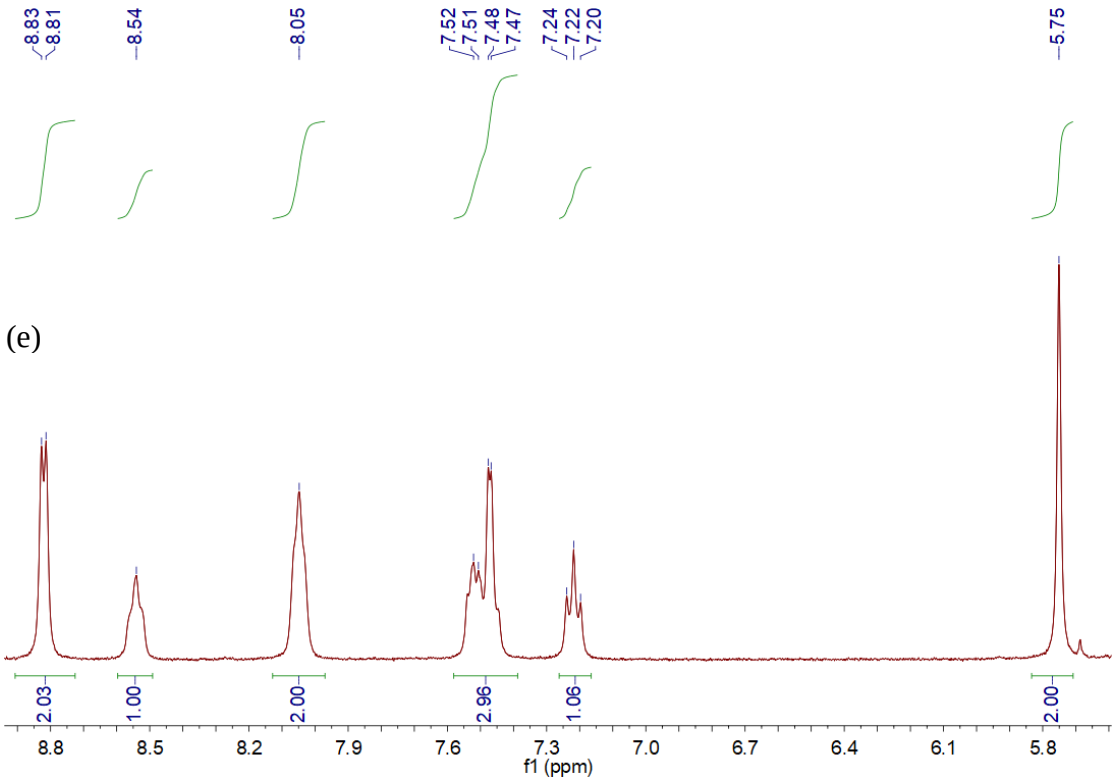
8.83
8.81
8.54
8.05
7.52
7.51
7.48
7.47
7.24
7.22
7.20
5.75
2.03
1.00
2.00
2.96
1.06
2.00
8.8
8.5
8.2
7.9
7.6
7.3
7.0
6.7
6.4
6.1
5.8
f1 (ppm)

(f)

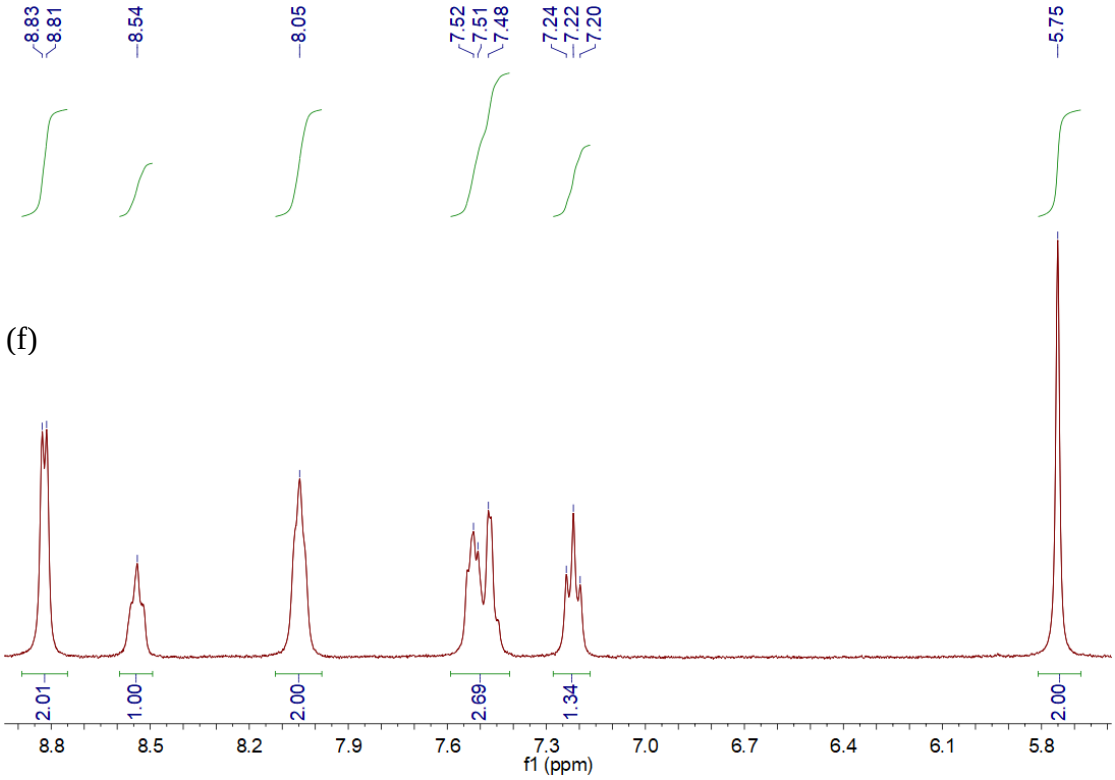
8.83
8.81
8.54
8.05
7.52
7.51
7.48
7.24
7.22
7.20
5.75
2.01
1.00
2.00
2.69
1.34
2.00
8.8
8.5
8.2
7.9
7.6
7.3
7.0
6.7
6.4
6.1
5.8
f1 (ppm)

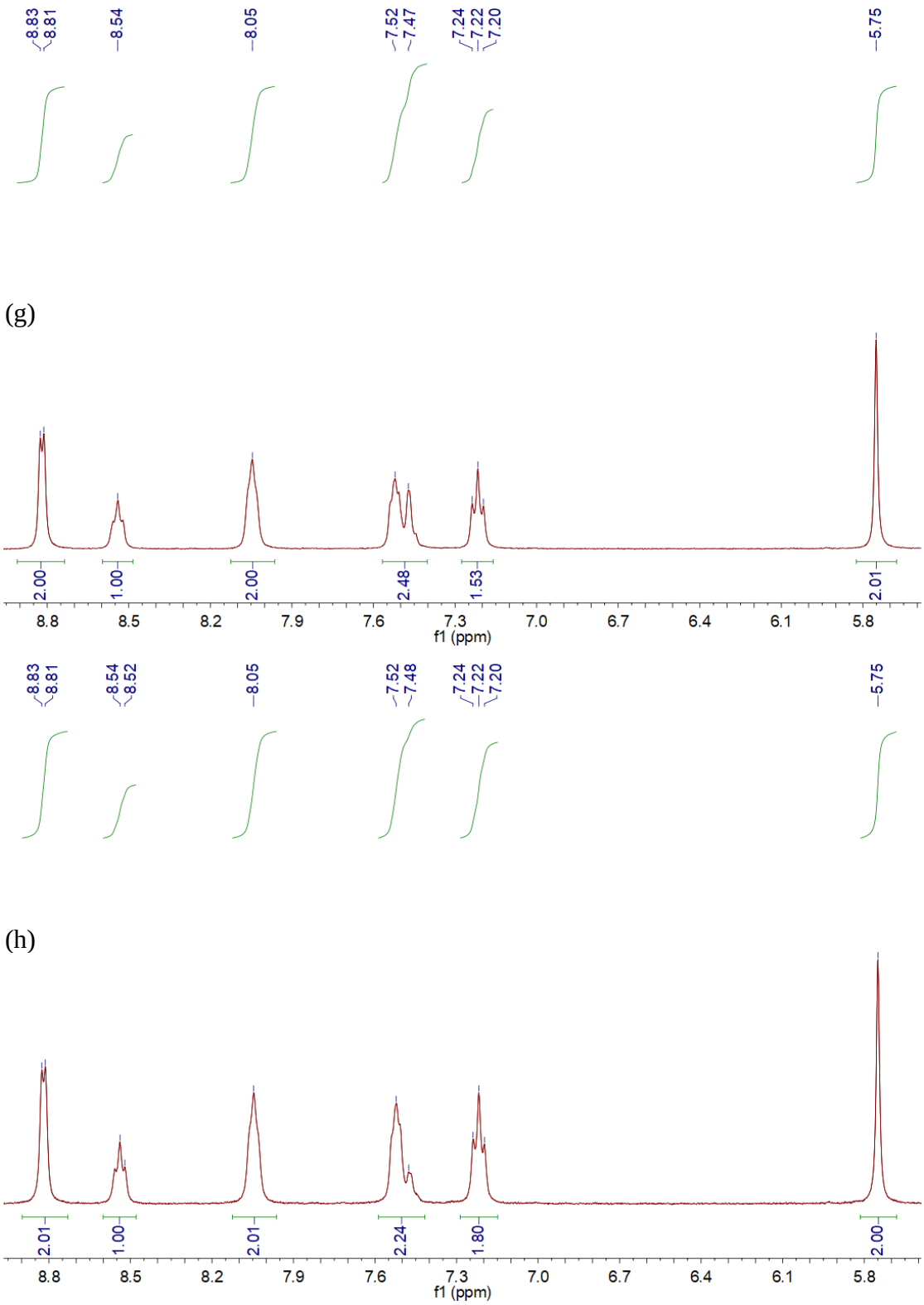

Fig. S3: ^{1}H NMR spectra of [F_xCl_{1-x}-BzPy][Ni(mnt)$_2$] with feed ratio of F to Cl is(a) 1:9, (b) 2:8, (c) 4:6, (d) 5:5, (e) 6:4, (f) 7:3, (g) 8:2, (h) 9:1.

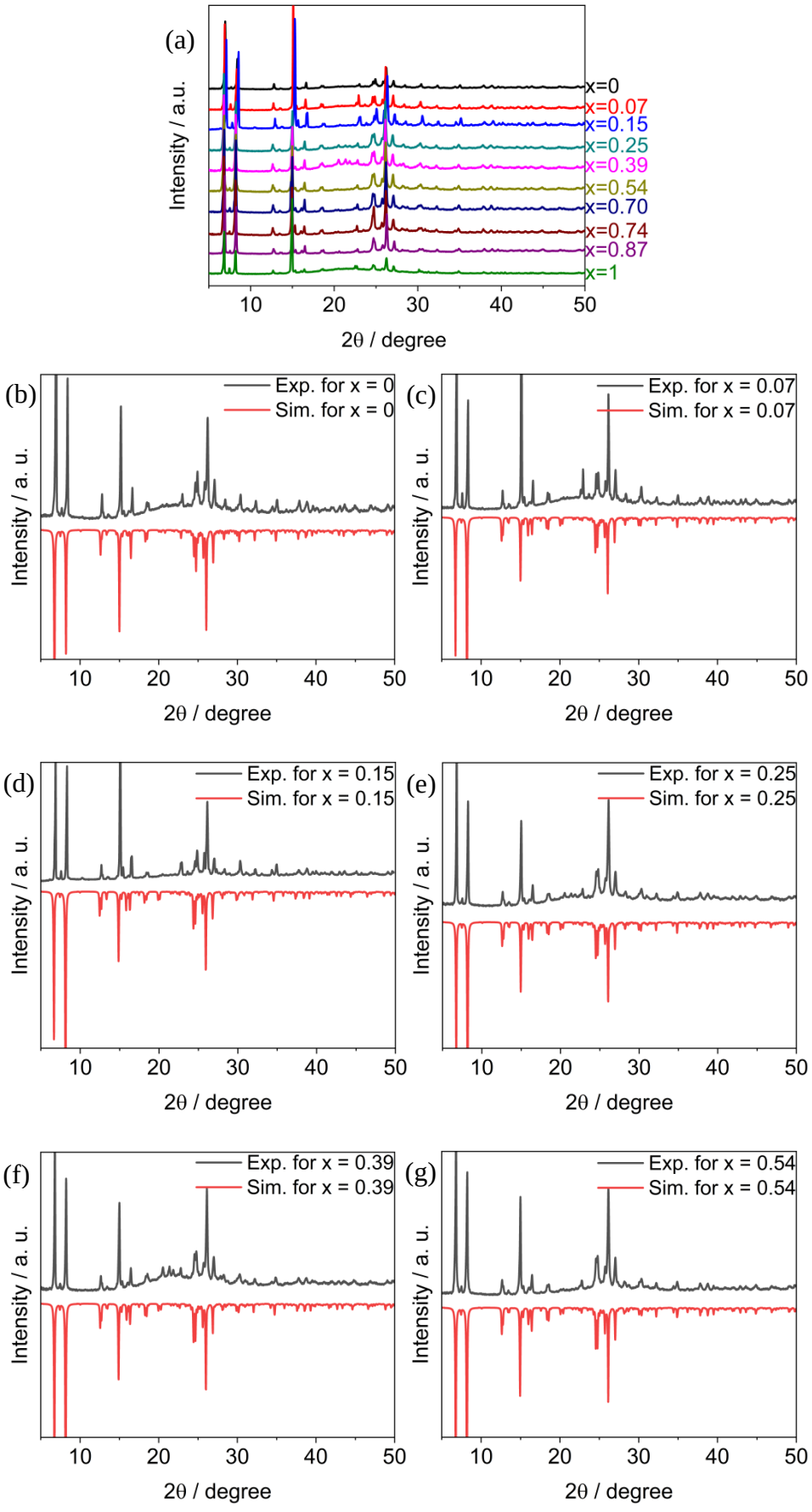
(a)
Intensity / a.u.
x=0
x=0.07
x=0.15
x=0.25
x=0.39
x=0.54
x=0.70
x=0.74
x=0.87
x=1
10
20
30
40
50
2θ / degree
(b)
Exp. for x = 0
Sim. for x = 0
Intensity / a. u.
2θ / degree
(c)
Exp. for x = 0.07
Sim. for x = 0.07
Intensity / a. u.
2θ / degree
(d)
Exp. for x = 0.15
Sim. for x = 0.15
Intensity / a. u.
2θ / degree
(e)
Exp. for x = 0.25
Sim. for x = 0.25
Intensity / a. u.
2θ / degree
(f)
Exp. for x = 0.39
Sim. for x = 0.39
Intensity / a. u.
2θ / degree
(g)
Exp. for x = 0.54
Sim. for x = 0.54
Intensity / a. u.
2θ / degree

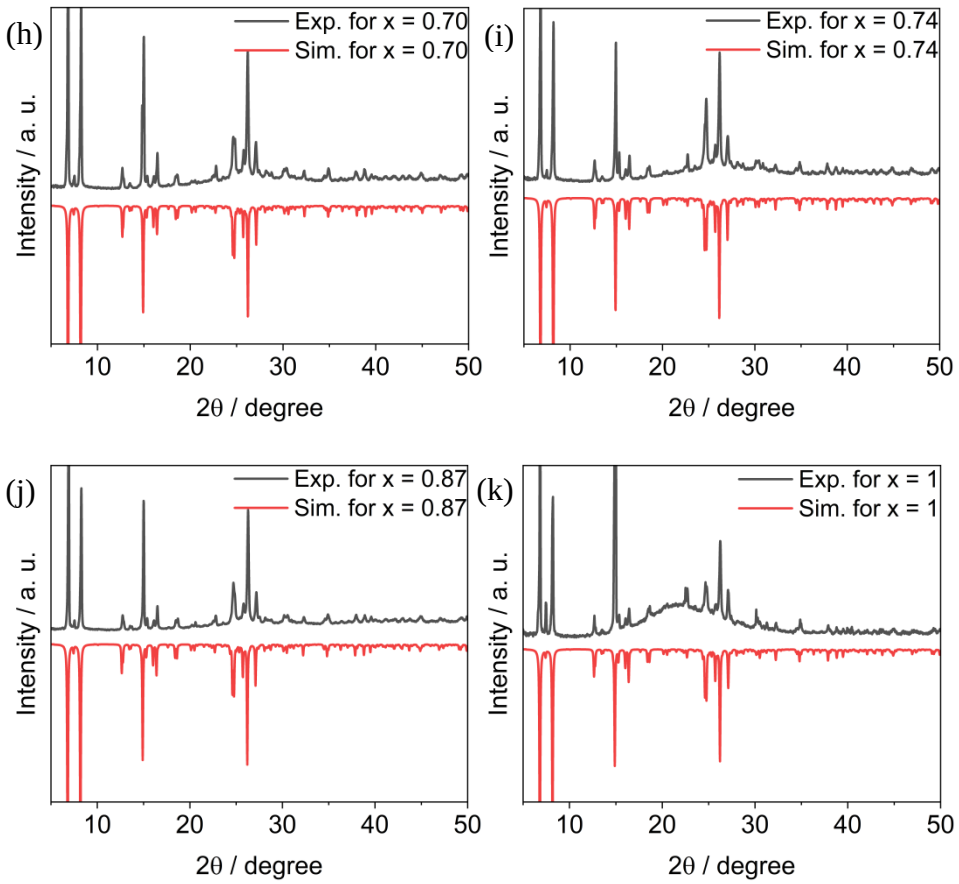

Fig. S4: (a) PXRD patterns of $[F_xCl_{1-x}\text{-BzPy}][Ni(mnt)_2]$ (x = 0–1). Experimental and simulated PXRD patterns of (b) x = 0, (c) x = 0.07, (d) x = 0.15, (e) x = 0.25, (f) x = 0.39, (g) x = 0.54, (h) x = 0.70, (i) x = 0.74, (j) x = 0.87, (k) x = 1, where the simulated PXRD pattern was obtained from the single crystal X-ray diffraction data using Mercury3.1 program.

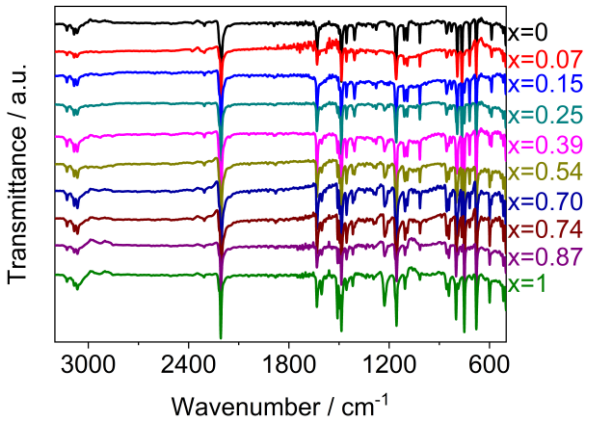

Fig. S5: IR spectra of $[F_xCl_{1-x}\text{-BzPy}][Ni(mnt)_2]$ (x = 0–1).

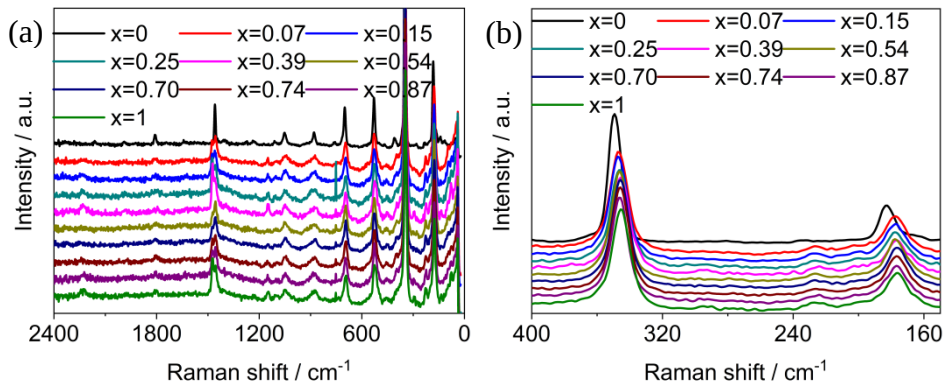

Fig. S6: Raman spectra of $[F_xCl_{1-x}\text{-BzPy}][Ni(mnt)_2]$ (x = 0–1) in the range of (a) 2400–21 cm^{-1} and (b) 400–150 cm^{-1}.

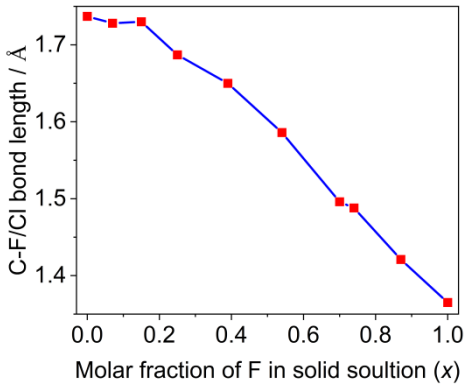

Fig. S7: C-F/Cl bond length with x in $[F_xCl_{1-x}\text{–BzPy}][Ni(mnt)_2]$ (x = 0–1).

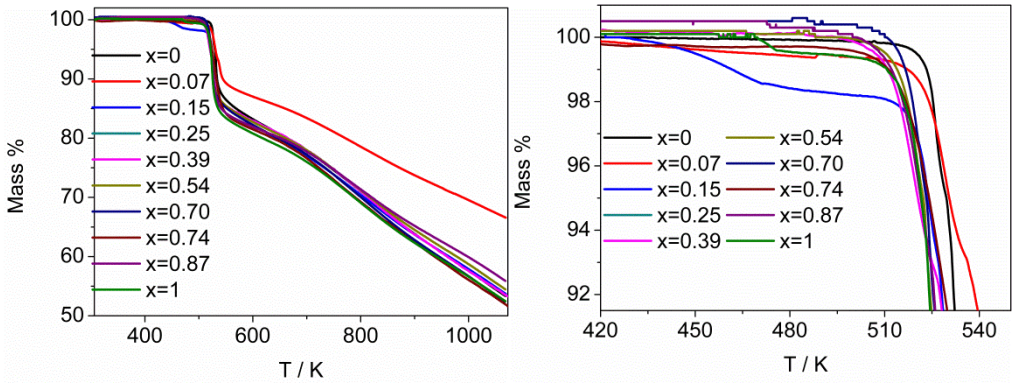

Fig. S8: TG plots of $[F_xCl_{1-x}\text{-BzPy}][Ni(mnt)_2]$ (x = 0–1) in 300–1073 K.

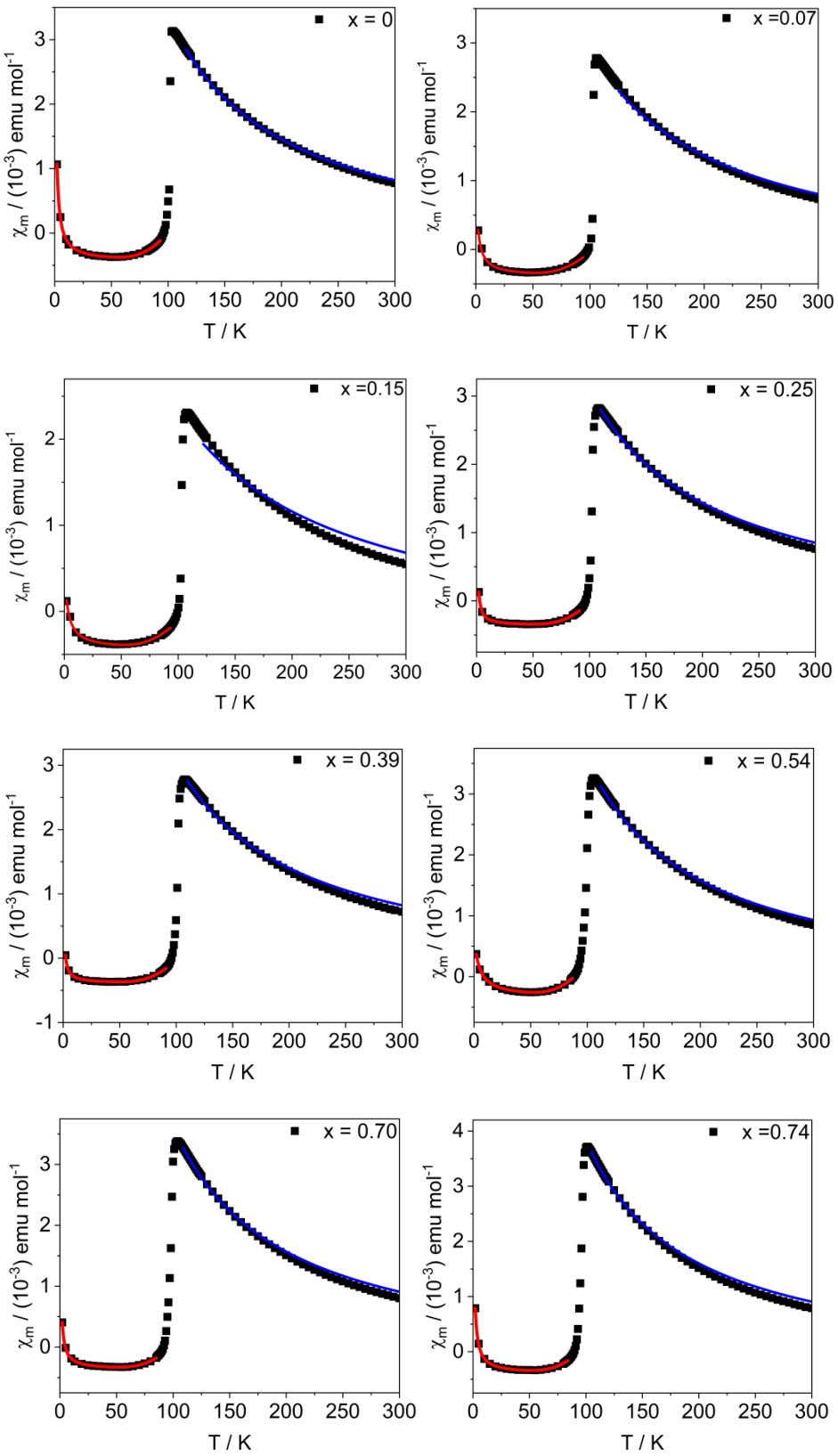
x = 0
x =0.07
x =0.15
x = 0.25
x = 0.39
x = 0.54
x = 0.70
x =0.74
χm / (10-3) emu mol-1
T / K

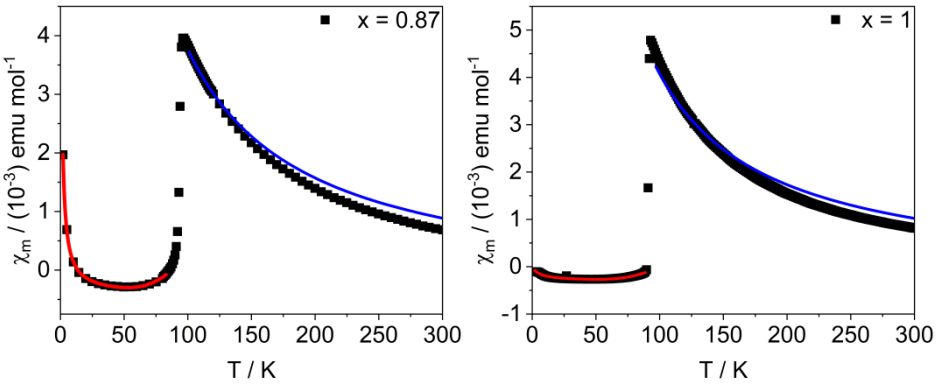

Fig. S9: Plots of χ_m–T for [F_xCl_{1-x}–BzPy][Ni(mnt)$_2$] (x = 0–1) in 2–300 K (the black squares represent the experimental data; the red and blue lines represent the theoretically reproduced curves and the details see the main text).

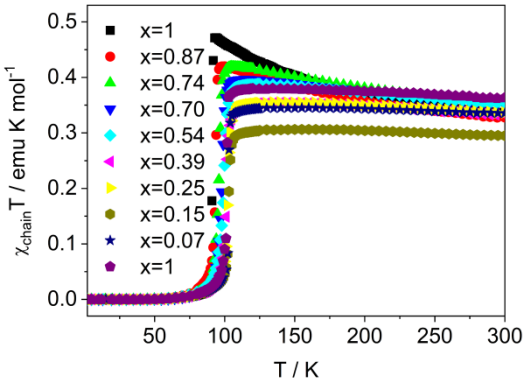

Fig. S10: Plots of $\chi_{chain}T$–T for [F_xCl_{1-x}–BzPy][Ni(mnt)$_2$] (x = 0–1), where χ_{chain} was acquired by χ_m subtracting the C/(T–θ) and χ_0 terms and these terms were obtained by fitting the χ_m in LTP (see Main text and Table S3).

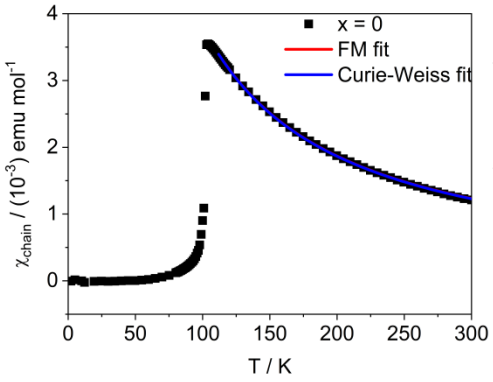
x = 0
FM fit
Curie-Weiss fit
χchain / (10-3) emu mol-1
T / K

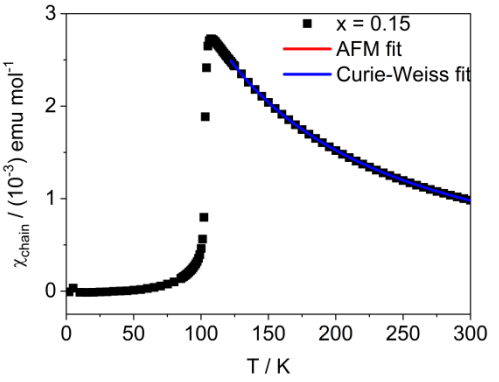
x = 0.15
AFM fit
Curie-Weiss fit
χchain / (10-3) emu mol-1
T / K

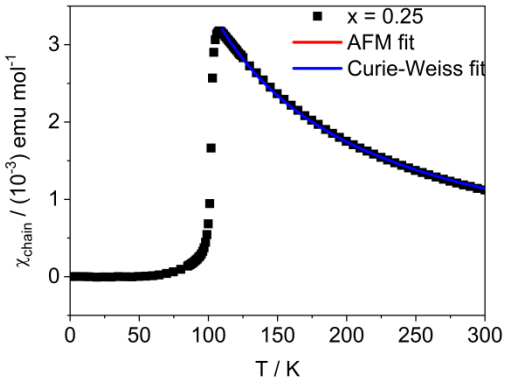
x = 0.25
AFM fit
Curie-Weiss fit
χchain / (10-3) emu mol-1
T / K

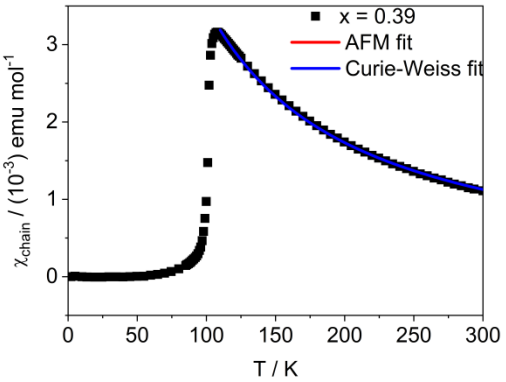
x = 0.39
AFM fit
Curie-Weiss fit
χchain / (10-3) emu mol-1
T / K

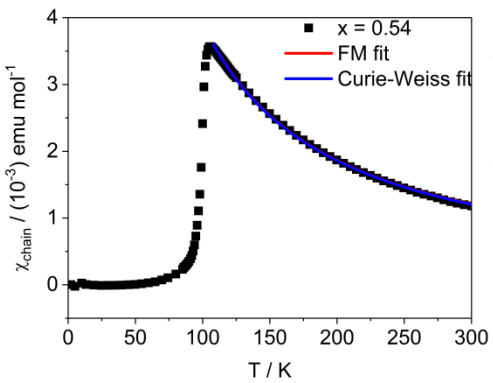
x = 0.54
FM fit
Curie-Weiss fit
χchain / (10-3) emu mol-1
T / K

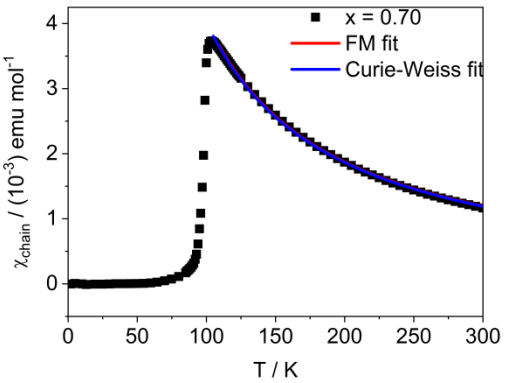
x = 0.70
FM fit
Curie-Weiss fit
χchain / (10-3) emu mol-1
T / K

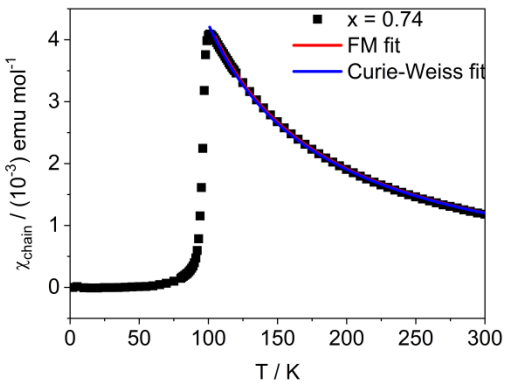
x = 0.74
FM fit
Curie-Weiss fit
χchain / (10-3) emu mol-1
T / K

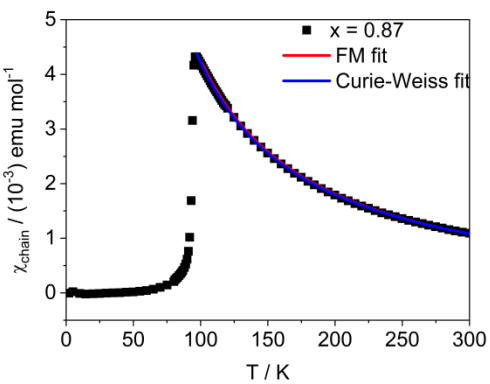
x = 0.87
FM fit
Curie-Weiss fit
χchain / (10-3) emu mol-1
T / K

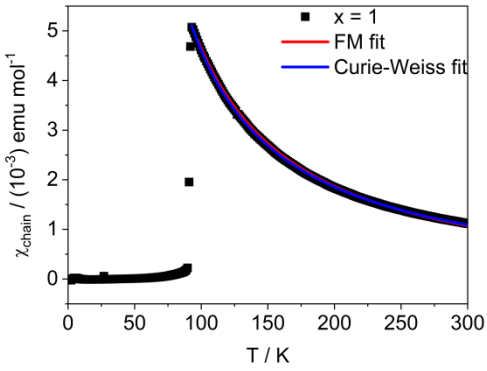

Fig. S11: Plots of χ_m–T for [F_xCl_{1-x}–BzPy][Ni(mnt)$_2$] (x = 0–1) in 2–300 K (the black squares represent the experimental data; the red and blue lines represent the theoretically reproduced curves in HTP and the parameters acquired from fit using Eq. (4) or Eq. (7) or Curie-Weiss law together with an additional χ_0 term, ref. main text and Table S5 and S6).

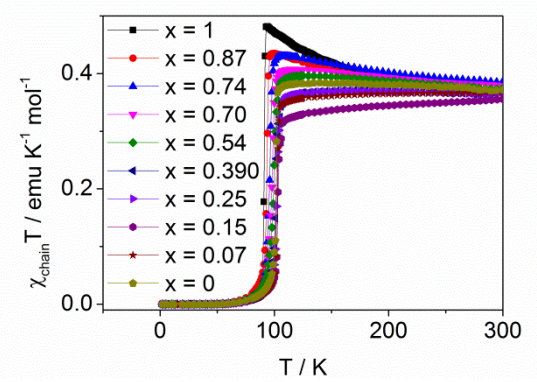

Fig. S12: Plots of $\chi_{chain}T$–T for [F_xCl_{1-x}–BzPy][Ni(mnt)$_2$] (x = 0–1), herein, each plot of χ_{chain}–T is the same as that in Fig. S11 for each salt, and the χ_{chain} was corrected by χ_0 obtained by fitting the χ_m in HTP using uniform S = ½ FM or AFM spin chain magnetic susceptibility equation with an additional χ_0 (see Main text and Table S5).

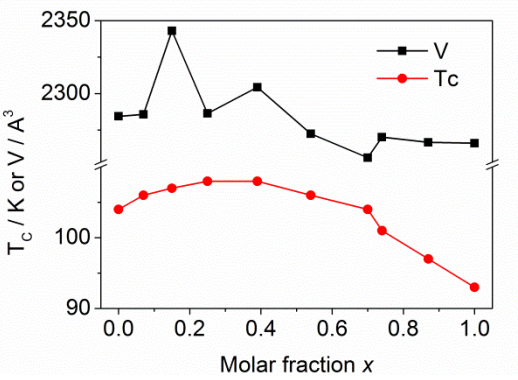

Fig. S13: Change of T_C and V with x in [F_xCl_{1-x}–BzPy][Ni(mnt)$_2$] (x = 0–1).

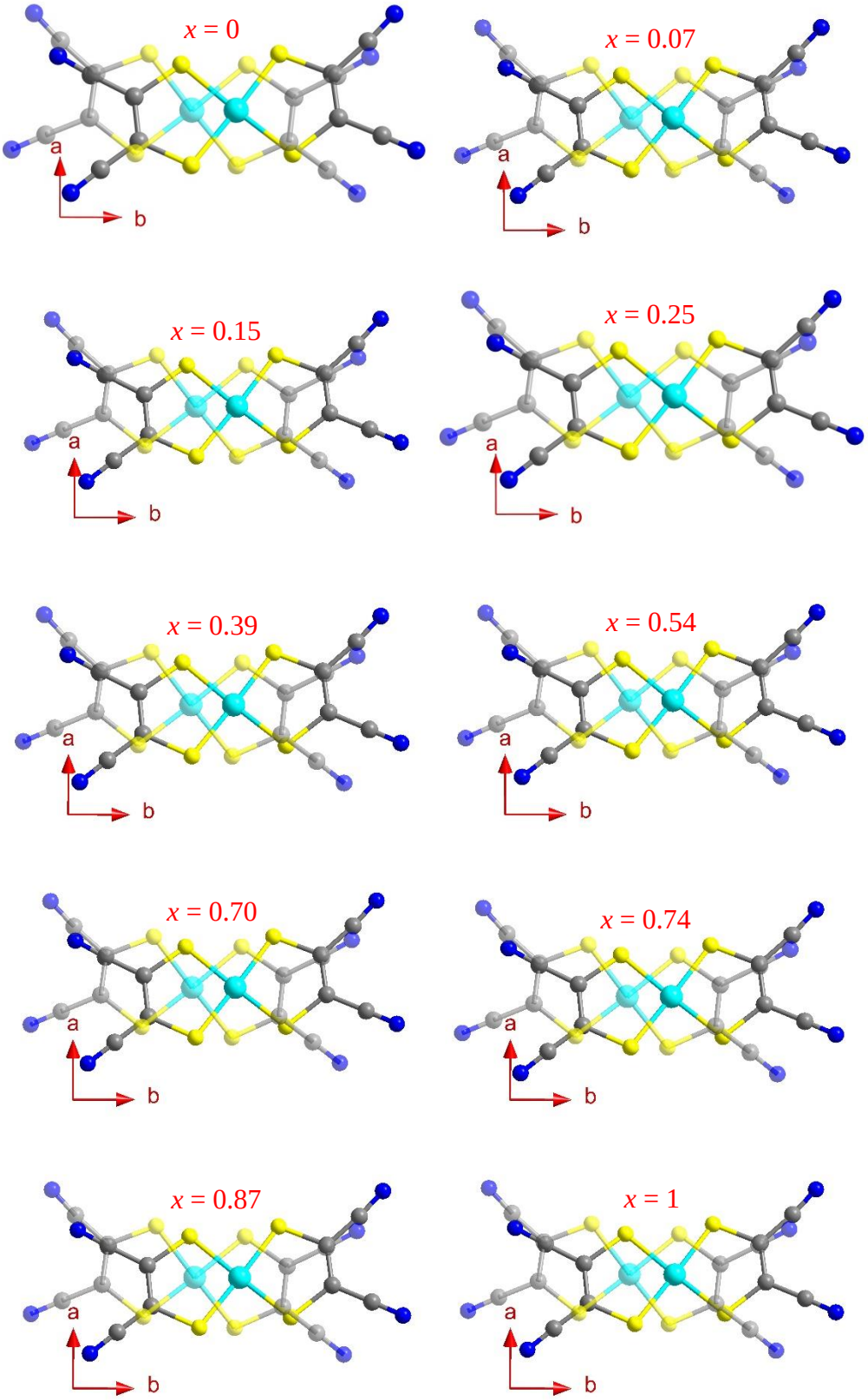

Fig. S14: The stacking mode of two superimposed anions in a stack of $[F_xCl_{1-x}\text{-BzPy}][Ni(mnt)_2]$ (x = 0–1).

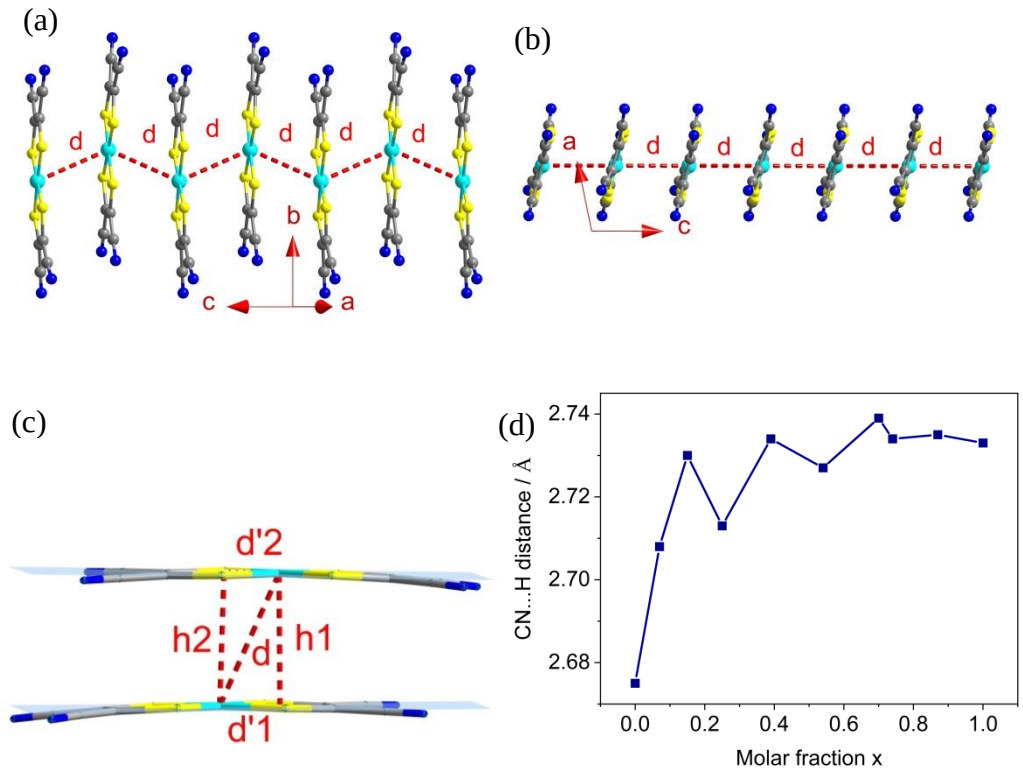

Fig. S15: Side views of an anion stack along (a, b) *a*+*c* and *b*-axis directions, respectively, showing the equal Ni…Ni distances of neighboring anions. (c) Side view of mean-molecule plane of $[Ni(mnt)_2]^-$ defined by four sulphur atoms. Plots of (d) CN…H distance with *x* in $[F_xCl_{1-x}\text{-BzPy}][Ni(mnt)_2]$ (x = 0–1).

Table S1: Crystallographic data for compounds $[F_xCl_{1-x}\text{-BzPy}][Ni(mnt)_2]$ (x = 0–1) at ambient temperature

x	0	0.07	0.15	0.25
Temp. / K	296(2)	293(2)	293(2)	293(2)
Wavelength / Å	0.71073	0.71073	0.71073	0.71073
Formula weight	543.74	542.54	541.30	539.69
Space group	$P2_1/c$	$P2_1/c$	$P2_1/c$	$P2_1/c$
CCDC no.	158525	2210261	2210274	2210275
Crystal system	Monoclinic	Monoclinic	Monoclinic	Monoclinic
a / Å	12.105(2)	12.108(2)	12.201(10)	12.1300(4)
b / Å	26.218(4)	26.230(5)	26.520(19)	26.1989(9)
c / Å	7.374(2)	7.3716(11)	7.410(6)	7.3663(2)
β / °	102.55(2)	102.496(5)	102.32(3)	102.4024(11)
V /Å^3, Z	2284.2(9), 4	2285.7(7), 4	2343(3), 4	2286.33(13), 4
ρ / g·cm^{-1}	1.581	1.577	1.535	1.568
μ / mm^{-1}	1.350	1.341	1.301	1.322
$F(000)$	1100	1098	1095	1092
θ Range for data collection (°)	1.89–25.00	2.319–25.499	2.297– 25.210	2.898–25.497
Index ranges	-14 ≤ h ≤ 14 -31 ≤ k ≤ 1 -1 ≤ l ≤ 8	-14≤h≤14 -31≤k≤31 -8≤l≤8	-14≤h≤14 -31≤k≤31 -8≤l≤8	-14 ≤ h ≤ 14 -31 ≤ k ≤ 31 -8 ≤ l ≤ 8
R_{int}	0.0455	0.0899	0.0956	0.0490
Reflect./restraints/parameters	3997 / 0 / 294	4241 / 0 / 281	4176 / 0 / 281	4248 / 0 / 281
Refinement method	Full-matrix least-squares on F^2	Full-matrix least-squares on F^2	Full-matrix least-squares on F^2	Full-matrix least-squares on F^2
Goodness of fit on F^2	1.023	1.031	1.019	1.107
R_1, wR_2[a] [$I>2\sigma$(I)]	0.0460, 0.1065	0.0352, 0.0716	0.0393, 0.1011	0.0387, 0.0791
R_1, wR_2[a] [all data]	0.0773, 0.1226	0.0585, 0.0779	0.0560, 0.1081	0.0509, 0.0830
Residual / e·Å^{-3}	0.457/-0.426	0.282/-0.348	0.512/-0.411	0.282/-0.342

Continue to Table S1

x	0.39	0.54	0.70	0.74
Temp. / K	293(2)	293(2)	293(2)	293(2)
Wavelength / Å	0.71073	0.71073	0.71073	0.71073
Formula weight	537.40	534.89	532.18	531.57
Space group	$P2_1/c$	$P2_1/c$	$P2_1/c$	$P2_1/c$
CCDC no.	2210276	2210277	2210278	2210282
Crystal system	Monoclinic	Monoclinic	Monoclinic	Monoclinic
a / Å	12.1691(17)	12.1259(5)	12.125(11)	12.1396(12)
b / Å	26.251(4)	26.0819(12)	25.88(2)	26.017(3)
c / Å	7.3843(9)	= 7.3514(3)	7.344(6)	7.3495(7)
β / °	102.348(5)	102.2104(12)	101.78(3)	102.038(4)
V /Å^3, Z	2304.3(6), 4	2272.40(17), 4	2256(3), 4	2270.1(4), 4
ρ / g·cm^{-1}	1.549	1.563	1.567	1.555
μ / mm^{-1}	1.297	1.298	1.289	1.277
F(*000*)	1088	1083	1078	1076
θ Range for data collection (°)	2.891–25.498	2.322–25.499	2.919–25.497	2.909–25.498
Index ranges	-14 ≤ h ≤ 14 -31 ≤ k ≤ 31 -8 ≤ l ≤ 8	-14 ≤ h ≤ 14 -31 ≤ k ≤ 31 -8 ≤ l ≤ 8	-14 ≤ h ≤ 14 -31 ≤ k ≤ 28 -8 ≤ l ≤ 8	-14 ≤ h ≤ 14 -31 ≤ k ≤ 31 -8 ≤ l ≤ 8
R_{int}	0.0821	0.1442	0.0562	0.0692
Reflect./restraints /parameters	4265 / 0 / 281	4232 / 0 / 281	4192 / 0 / 281	4226 / 0 / 281
Refinement method	Full-matrix least-squares on F^2	Full-matrix least-squares on F^2	Full-matrix least-squares on F^2	Full-matrix least-squares on F^2
Goodness of fit on F^2	1.074	1.044	1.159	1.136
R_1, wR_2[a] [$I>2\sigma$(I)]	0.0530, 0.0988	0.0426, 0.0929	0.0703, 0.1097	0.0614, 0.0958
R_1, wR_2[a] [all data]	0.0796, 0.1055	0.0777, 0.1030	0.0999, 0.1160	0.0865, 0.1015
Residual / e·Å^{-3}	0.316/ -0.438	0.245/-0.322	0.559/-0.543	0.423/-0.506

Continue to Table S1

x	0.87	1
Temp. / K	293(2)	293(2)
Wavelength / Å	0.71073	0.71073
Formula weight	529.47	527.29
Space group	$P2_1/c$	$P2_1/c$
CCDC no.	2210273	182194
Crystal system	Monoclinic	Monoclinic
a / Å	12.1411(5)	12.1500(4)
b / Å	25.9867(11)	25.9523(6)
c / Å	7.3406(3)	7.3397(3)
β / °	101.8663(14)	101.74
V /Å^3, Z	2266.52(16), 4	2265.95(13), 4
ρ / g·cm^{-1}	1.552	1.546
μ / mm^{-1}	1.265	1.251
F(*000*)	1072	1068
θ Range for data collection (°)	2.910–25.494	1.57–25.05
Index ranges	-14 ≤ h ≤ 14 -31 ≤ k ≤ 31 -8 ≤ l ≤ 8	-14≤h≤12 -19≤k≤30 -8 ≤ l ≤ 8
R_{int}	0.0418	0.0436
Reflect./restraints /parameters	4217 / 0 / 281	4013 / 0 / 281
Refinement method	Full-matrix least-squares on F^2	Full-matrix least-squares on F^2
Goodness of fit on F^2	1.148	1.046
R_1, wR_2[a] [$I>2\sigma$(I)]	0.0482, 0.0934	0.0619, 0.1535
R_1, wR_2[a] [all data]	0.0614, 0.0970	0.0994, 0.1804
Residual / e·Å^{-3}	0.346/-0.419	0.879/-0.659

Table S2: Coordinated bond lengths (Å) and angles (°) in an anionic moiety for $[F_xCl_{1-x}–BzPy][Ni(mnt)_2]$ (x = 0–1)

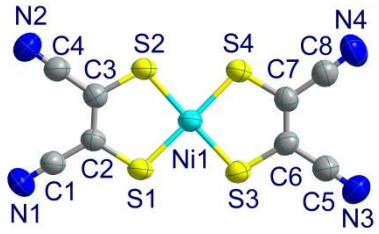

x	Ni−S1	Ni−S2	Ni−S3	Ni−S4	S1−Ni−S2	S3−Ni−S4
0	2.1447(12)	2.1392(12)	2.1510(12)	2.1395(12)	92.17(5)	92.37(5)
0.07	2.1436(8)	2.1409(8)	2.1531(8)	2.1409(8)	92.15(3)	92.41(3)
0.15	2.1651(14)	2.1628(14)	2.1745(14)	2.1604(14)	91.96(7)	92.24(7)
0.25	2.1457(8)	2.1423(8)	2.1551(8)	2.1405(8)	92.18(3)	92.43(3)
0.39	2.1530(11)	2.1486(11)	2.1618(11)	2.1468(11)	92.13(4)	92.38(4)
0.54	2.1395(9)	2.1394(9)	2.1489(9)	2.1394(10)	92.23(4)	92.41(4)
0.70	2.141(2)	2.134(2)	2.146(2)	2.134(2)	92.61(9)	92.89(9)
0.74	2.1446(12)	2.1411(12)	2.1526(12)	2.1396(12)	92.24(5)	92.45(5)
0.87	2.1435(10)	2.1417(10)	2.1537(10)	2.1391(10)	92.24(4)	92.42(4)
1	2.1454(14)	2.1441(14)	2.1516(14)	2.1412(15)	92.27(6)	92.46(6)

Table S3: The parameters (α, Δ/k_B, C and θ) obtained by fitting the temperature dependent magnetic susceptibilities in LTP

x	0	0.07	0.15	0.25	0.39
α	17(4)	6(2)	5(2)	13(2)	13(3)
Δ/k_B / K	598(23)	526(33)	517(42)	591(17)	586(23)
C / (10^{-3}) emu K mol^{-1}	3.70(9)	2.66(8)	2.76(5)	1.02(4)	1.06(6)
θ / K	−0.4(1)	−1.9(3)	−2.8 (4)	−0.1(1)	−0.4(2)
χ_0 / (10^{-4}) emu mol^{-1}	−4.49(5)	−3.93(7)	−4.44(9)	−3.64(2)	−3.92(3)
Temp. range / K	2−93	2−93	2−93	2−91	2−91
x	0.54	0.70	0.74	0.87	1
α	12(6)	12(4)	11(4)	10(6)	7(3)
Δ/k_B / K	544(42)	571(27)	541(34)	508(45)	551(34)
C / (10^{-3}) emu K mol^{-1}	4.58(5)	1.94(5)	2.93(9)	6.06(7)	1.76(2)
θ / K	−4.4(5)	−0.5(1)	−0.5(1)	−0.5(1)	−6 (1)
χ_0 / (10^{-4}) emu mol^{-1}	−3.47(1)	−3.70(3)	−4.04(5)	−4.26(9)	−3.01(5)
Temp. range / K	2−87	2−85	2−84	2−83	2−89

Table S4: The parameter J/k_B and temperature range of fitted susceptibility data in HTP

x	0	0.07	0.15	0.25	0.39
J/k_B / K	0.4(8)	-11.5(7)	-27.5(±1.3)	-6.7(4)	-7.2(4)
Temp. range / K	112−300	125−300	122−300	110−300	110−300
x	0.54	0.70	0.74	0.87	1
J/k_B / K	1.5(7)	2.8(6)	5.9(6)	4.9(5)	7.8(4)
Temp. range / K	108−300	105−300	101−300	97−300	93−300

Table S5: The parameter J/k_B and temperature range of fitted susceptibility data in HTP

x	0	0.07	0.15	0.25	0.39
J/k_B / K	1.2(±2.4)	-4.3(1)	-13.3(1)	-2.9(2)	-2.8(1)
Temp. range / K	112−300	125−300	122−300	110−300	110−300
x	0.54	0.70	0.74	0.87	1
J/k_B / K	3.1(±1.8)	4.9(±1.6)	8.4(±1.5)	9.8(±1.2)	15.9(4)
Temp. range / K	108−300	105−300	101−300	97−300	93−300

Table S6: The parameter θ and temperature ranges of susceptibility data fitted in HTP

x	0	0.07	0.15	0.25	0.39
θ / K	2.5(2)	-5.7(1)	-17.1(1)	-3.9(3)	-3.8(3)
Temp. range / K	112−300	125−300	122−300	110−300	110−300
x	0.54	0.70	0.74	0.87	1
θ / K	5.8(3)	8.9(3)	14.1(2)	15.8(1)	23.0(1)
Temp. range / K	108−300	105−300	101−300	97−300	93−300